

## Burnup Adaptation Model in STREAM/RASTK Code System

Peng Zhang, Jiwon Choi, Sooyoung Choi, Deokjung Lee\*  
Department of Nuclear Engineering, UNIST, 50 UNIST-gil, Ulsan, 44919  
Corresponding author: deokjung@unist.ac.kr;

### 1. Introduction

The burnup adaptation (BUA) model has been developed for the STREAM/RASTK code system to reduce the biases and uncertainties of predicted core characteristics parameters by using information of power distribution from the reference like the in-core detector system. It can be applied to the modeling of the reactor core at any time when the reference like measured data is available.

During the operation of a nuclear power plant, it is very important to have an accurate prediction of the reactor parameters. However, in practice, the plant operation condition may change due to some unknown reason. It is impossible to quantify the effects and have them considered in the calculations. This will result in the departure of the prediction data from the actual (operation) data and will cause error/bias for the following modeling and operation of the plant.

The idea of BUA is that the computed power distribution is sensitive to the spatial distribution of assembly reactivity errors, which is sensitive to the distribution of the assembly burnups. In addition, the change of the plant operating condition will cause a change in the power distribution, which will then cause a change in the burnup distribution. Therefore, by adjusting the assembly burnups, it is possible to produce a better agreement between the calculated and reference power distributions, which is a compensation of the unknown operation condition change in the modeling.

### 2. Methods and Results

#### 2.1. The burnup adaptation model

##### 2.1.1. The burnup adjustment method

The burnups (BUs) of the fuel assemblies (FAs) are modified as follows:

$$BU_{new}(I_z) = BU_{old}(I_z) \cdot M_B \cdot (M_z \cdot S(I_z) + 1.0), \quad (1)$$

where  $M_B$  and  $M_z$  are the two factors used to adjust the burnup of the FA,  $I_z$  is the axial node index and  $S$  is the shape function that is used to adjust the axial BU distribution and is fixed as a sine-like shape as shown in Fig. 1.

The micro-depletion approach is adopted in RAST-K for the core depletion analysis. Therefore, once the BUs

are modified, the corresponding nuclide number densities (NDs) of the nodes should also be changed to be consistent with the BUs. The new NDs are obtained by interpolating the NDs which are read from the cross-section table and are obtained with the lattice code as follows:

$$ND_{new} = ND_{old} - (ND_{Table,old} - ND_{Table,new}), \quad (2)$$

where  $ND_{Table,old}$  and  $ND_{Table,new}$  are the NDs corresponding to the original and the modified BUs, respectively.

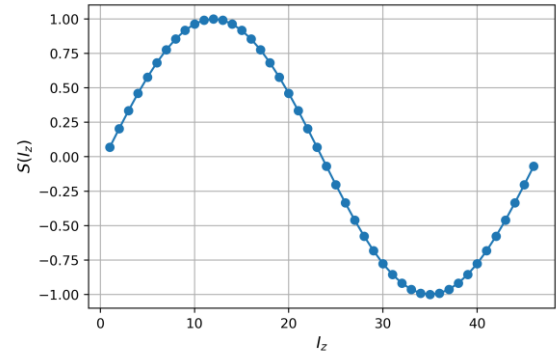


Figure 1. The shape function  $S(I_z)$ .

##### 2.1.2. The optimization method

The optimization target of the BUA is to find the factors  $M_B$  and  $M_z$  for every FA that is chosen to be adjusted. It is to find the minimum value for the following function:

$$G(\mathbf{x}) = \begin{bmatrix} RMSE(\mathbf{x}) + 0.001 |CBC_{ref} - CBC(\mathbf{x})| \\ |ASI_{ref} - ASI(\mathbf{x})| \end{bmatrix}, \quad (3)$$

where  $\mathbf{x}$  contains the factors:

$$\mathbf{x} = \begin{bmatrix} M_B \\ M_z \end{bmatrix}. \quad (4)$$

RMSE stands for the root mean square error, which is the error between the calculated and reference 2D radial power distributions. CBC is the critical boron concentration and  $CBC_{ref}$  is from the reference data. ASI stands for the axial shape index, which is a number

representing the axial power distribution, and  $ASI_{ref}$  is from the reference data.

The optimization objective is to minimize:

$$F(\mathbf{x}) = \frac{1}{2} \mathbf{G}^T(\mathbf{x}) \mathbf{G}(\mathbf{x}) = \frac{1}{2} \left[ \begin{array}{l} (RMSE(\mathbf{x}) + 0.001 |CBC_{ref} - CBC(\mathbf{x})|)^2 \\ + (ASI_{ref} - ASI(\mathbf{x}))^2 \end{array} \right] \quad (5)$$

With initial guess  $\mathbf{x}^{(0)}$ , the vector  $\mathbf{x}$  can be updated as:

$$\begin{aligned} \mathbf{x}^{(1)} &= \mathbf{x}^{(0)} - \gamma_0 \nabla F(\mathbf{x}^{(0)}) \\ &= \mathbf{x}^{(0)} - \gamma_0 J_G(\mathbf{x}^{(0)})^T G(\mathbf{x}^{(0)}), \end{aligned} \quad (6)$$

where  $\gamma_0$  is the learning rate and  $J_G$  is the Jacobian matrix. To get the Jacobian matrix  $J_G$ , three tests with different  $\mathbf{x}$  are run first to get the initial  $J_G$ , and then it is updated for every iteration by solving the following equation:

$$\begin{aligned} J_G(\mathbf{x}^{(0)}) (\mathbf{x}^{(1)} - \mathbf{x}^{(0)}, \mathbf{x}^{(2)} - \mathbf{x}^{(0)}) \\ = (G(\mathbf{x}^{(1)}) - G(\mathbf{x}^{(0)}), G(\mathbf{x}^{(2)}) - G(\mathbf{x}^{(0)})). \end{aligned} \quad (7)$$

## 2.2. The numerical results

### 2.2.1. Description of the cases

A typical OPR1000 core has been modeled for 3 cycles. Three cases have been considered: 1) 100% power level for 3 cycles is assumed; 2) 80% power level is assumed for Cycle 2; and 3) the calculation parameters are the same as in case 1), while the BUA is applied in addition. Case 1) is referred to as the normal calculation without BUA. Case 2), with the operating condition change in Cycle 2, is referred to as the reference case. The Cycle 3 results of cases 1) and 2) would show big differences, while it is expected that the results of case 3) would be much closer to the reference case 2).

### 2.2.2. The sub-batch grouping

In the current BUA model, we consider the sub-batch-wise BUA, that is, several FAs in the same sub-batch will share the same  $M_B$  and  $M_Z$  factors.

Fig. 2 shows the loading pattern (LP) of this OPR1000 quarter core at Cycle 3 (OPR1000\_C3). Table 1 shows the information of the FAs in the core and the sub-batch grouping. The division of the sub-batches is mainly determined by the burning cycle and the number of FAs of the same type.

The BUA factors,  $M_B$  and  $M_Z$ , are first optimized for sub-batch 1, while the BUs for all the other FAs remain the same. After this optimization, the new BUs of sub-batch 1 FAs remain, and the optimization for sub-batch 2 follows. The optimization goes on sequentially until all the sub-batches are completed.

3	6	18	8	12	12	16	13	R
6	8	6	18	9	10	17	3	R
18	6	11	12	7	18	15	5	R
8	18	12	18	8	12	13	R	R
12	9	7	8	18	14	3	R	
12	10	18	12	14	6	R	R	
16	17	15	13	3	R	R		
13	3	5	R	R	R			
R	R	R	R					

Figure 2. The LP of the OPR1000\_C3 (R: reflector).

Table 1. The sub-batch grouping of the FAs.

LP	Number of FAs	Burning Cycle	Sub-batch
3	4.25	3rd	2
5	2	3rd	2
6	4	3rd	2
7	2	3rd	2
8	4	2nd	1
9	2	2nd	1
10	2	2nd	1
11	1	2nd	1
12	6	2nd	1
13	3	1st	3
14	2	1st	3
15	2	1st	3
16	1	1st	3
17	2	1st	3
18	7	1st	3
<b>Sum</b>	44.25	--	--

### 2.2.3. The search curve for the BUA factors

As an illustration of the effects of the BUA factors,  $M_B$  and  $M_Z$ , a test run is done with different factors for sub-batch 1 FAs. The changes of RMSE, CBC, and ASI are shown in Figs. 3-5. The results show that the RMSE and CBC are very sensitive to  $M_B$ , the factor that is mainly used to adjust the average BUs of the FAs and the radial BU profile, while they are not so sensitive to  $M_Z$ , the factor that is mainly used to adjust the axial BU profile. The results also show that the ASI is sensitive to both  $M_B$  and  $M_Z$ .

### 2.2.4. The results of OPR1000\_C3

The BUA is applied to OPR1000\_C3 at BOC (BU = 0.0 GWd/MT). The 2D radial power distribution and

ASI as well as CBC from the reference case are used as the optimization targets. The axial and radial power distribution changes are shown in Figs. 6 and 7. The radial power RMSE with BUA decreases compared to the normal calculation without BUA. The axial power profile with BUA is very close to the reference. Fig. 8 shows the CBC curve of the different cases, and the CBC results with BUA is much closer to the reference than without BUA. Fig. 9 shows the RMSE of the whole cycle, and the results with BUA are always below those of without BUA. The improvement to the ASI is tremendous, as shown in Fig. 10. The ASI changes during the whole cycle are very close to the reference although the BUA is only applied at BOC.

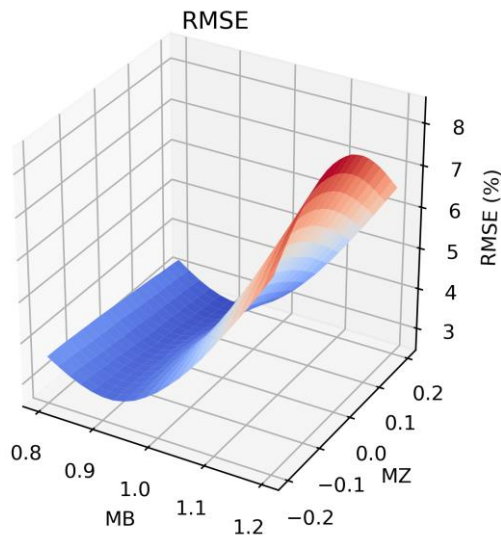


Figure 3. The change of RMSE with different  $M_B$  and  $M_Z$  for sub-batch 1 FAs.

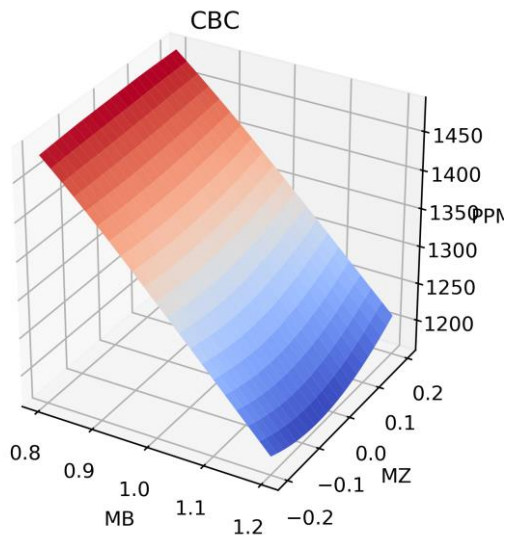


Figure 4. The change of CBC with different  $M_B$  and  $M_Z$  for sub-batch 1 FAs.

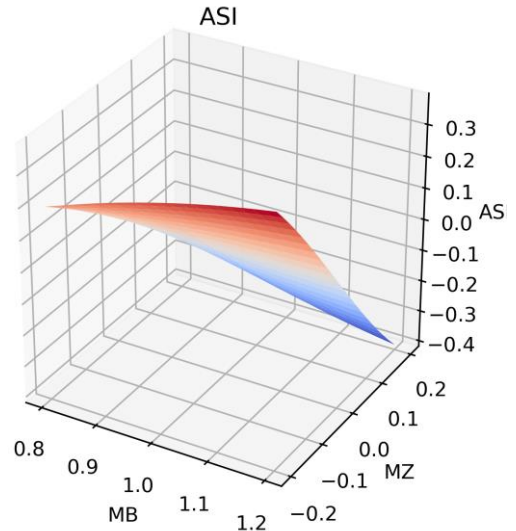


Figure 5. The change of ASI with different  $M_B$  and  $M_Z$  for sub-batch 1 FAs.

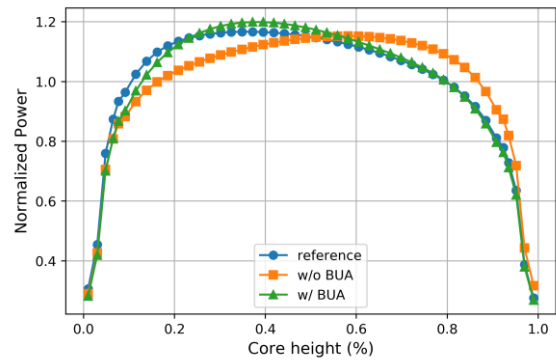


Figure 6. The axial power profiles of the OPR1000 core at BOC of Cycle 3.

-5.90	-5.48	-1.53	-3.74	-5.05	-2.91	3.88	6.42
-5.31	-4.75	-1.66	-0.19	0.40	1.33	1.16	0.66
-5.48	-4.49	-3.35	-1.42	-3.73	-1.47	4.28	3.74
-4.75	-2.76	-2.75	-0.44	1.27	1.53	1.09	-1.13
-1.53	-3.35	-4.58	-3.20	-1.11	2.64	5.38	5.73
-1.66	-2.76	-2.75	-1.48	-0.06	1.03	1.00	0.41
-3.74	-1.42	-3.20	0.10	-0.85	0.33	5.44	
-0.19	-0.45	-1.48	-0.17	0.68	0.65	0.79	
-5.05	-3.73	-1.11	-0.85	3.05	4.32	3.17	
0.39	1.26	-0.06	0.68	0.81	0.51	-1.14	
-2.91	-1.47	2.64	0.33	4.31	2.81		-5.90
1.32	1.52	1.03	0.65	0.51	-1.39		-5.31
3.87	4.28	5.38	5.43	3.17			6.42
1.15	1.09	0.99	0.78	-1.14			1.53
6.42	3.74	5.73					3.84
0.66	-1.13	0.40					1.68
					w/o BUA (%)		
					w/ BUA (%)		
						Min	
						Max	
						RMS	

Figure 7. The radial power differences from the reference case of the OPR1000 core at BOC of Cycle 3.

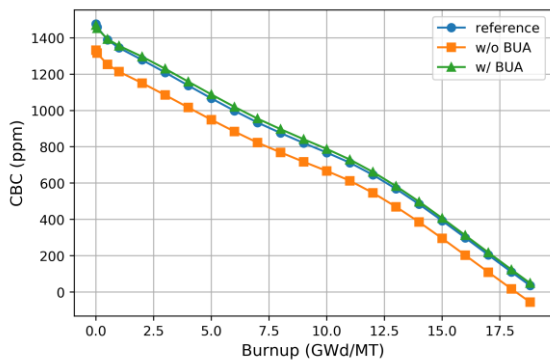


Figure 8. The CBC curve of the OPR1000 core for different cases.

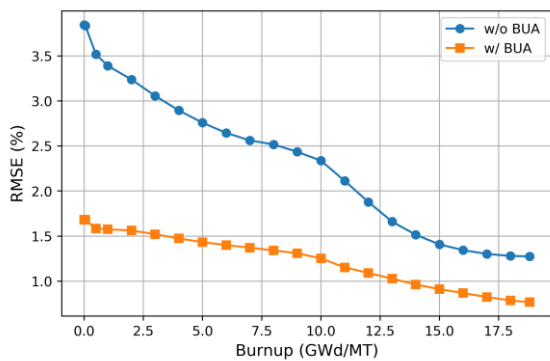


Figure 9. The RMSE changes of the OPR1000 core at Cycle 3 with and without BUA.

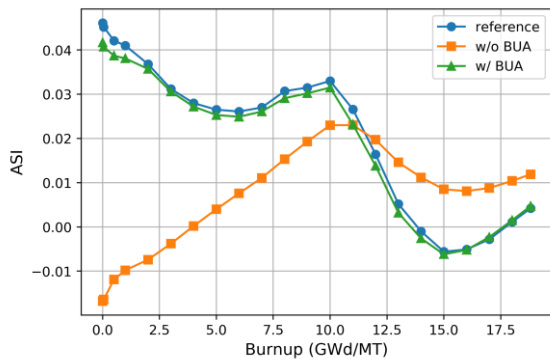


Figure 10. The ASI changes of the OPR1000 core at Cycle 3 for different cases.

### 3. Conclusions

A burnup adaptation model has been developed in the STREAM/RASTK 2-step code system. It can be used to compensate the modeling biases in the practical application of the actual operating core analysis. The 2D radial power distribution and ASI as well as the CBC from the reference, like the real-time in-core detector system, can be utilized as the optimization target. The numerical results of a typical OPR1000 core successfully demonstrate the capability of this burnup adaptation technique.

Further investigation will be conducted on the optimization problem, like the simultaneous optimization of the factors for all the sub-batches instead of the current sequential process, and the possible automatic sub-batch grouping using machine learning instead of the current manual grouping.

### ACKNOWLEDGMENT

This research was supported by the project (L17S018000) by Korea Hydro & Nuclear Power Co. Ltd..

### REFERENCES

- [1] K. S. Smith, et al., Benchmarks for Quantifying Fuel Reactivity Depletion Uncertainty, EPRI, Palo Alto, CA, 1022909, 2011.
- [2] D. Lancaster, Utilization of the EPRI Depletion Benchmarks for Burnup Credit Validation, EPRI, Palo Alto, CA, 1025203, 2012.
- [3] Elliot M. Sykora, Testing the EPRI Reactivity Depletion Decrement Uncertainty Methods, Master's thesis, MIT, 2015.
- [4] Geoffrey A. Gunow, LWR Fuel Reactivity Depletion Verification Using 2D Full Core MOC and Flux Map Data, Master's thesis, MIT, 2015.